Looking for Axion Like Particles in LDMX

Sophie Middleton

June 2024

1 Motivations

Axions are hypothetical particles that have the potential to solve the strong CP problem and are possible dark matter candidates. Axion-like particles (ALPs) are similar to the axion but do not necessarily solve the strong CP problem. ALPs are very light, weakly interacting particle that couple to photons. They are predicted by many beyond Standard Model theories [1] and are cold dark matter candidates. ALPs can couple to photons and electrons [2]:

$$\mathcal{L} \subset \frac{1}{4\Lambda_\gamma} a F_{\mu\nu} F^{\mu\nu} + \frac{\partial_\mu a}{\Lambda_e} \bar{e} \gamma_\mu \gamma_5 e \tag{1}$$

To understand the LDMX sensitivity to these particles we consider the photon and electron couplings to be independent and investigate the limiting cases where only one of the two interactions dominates. We focus on the photon case and imagine using the HCAL as the primary mode of identifying such events. To make this possible, there is a need to ensure good photon/neutron separation in the HCAL to improve sensitivity to ALP photon decay and discriminate against dominant backgrounds. In the HCAL, the main background to the ALP search will likely arises from photo-nuclear (PN) events, in particular those in which a neutron mimics a photon shower. The sensitivity of LDMX to visibly decaying ALPs is thus directly related to the neutron/photon separation power.

2 Realistic ALP Signatures and simulations

There are two dominant ALP production processes that can take place within LDMX:

1. The dominant **Primakoff production:** ALP produced via secondary photons interacting with the nuclei in the target (and elsewhere):

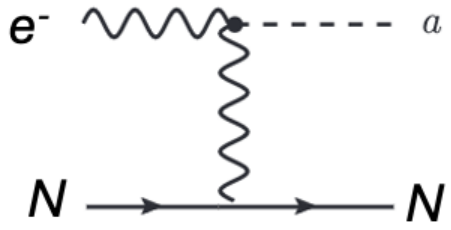

2. The sub-dominant **photon fusion production:** ALP produced from photons produced from the 8 GeV electrons in the target:

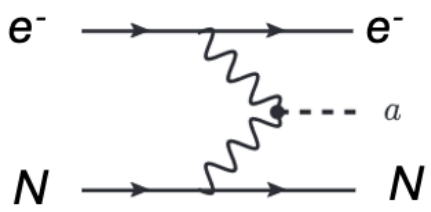

MadGraph v4 [3] was used to simulate ALPs production from these two processes within the target. A fiducial coupling of $g_{a\gamma} = 10^{-3} GeV^{-1}$ is used, where $g_{a\gamma} = \frac{1}{\Lambda_\gamma}$. The ALP is forced to decay to photons in both cases. ALP masses of $m_{ALP} = 10, 50, 100, 150, 200, 300, 400, 500$ MeV/c^2 are simulated. In MadGraph the other important ingredient is the model for the nucleus. We took a tungsten nucleus with a form factor used in appendix A of https://arxiv.org/pdf/0906.0580.

Table 1 lists the cross-sections derived by MadGraph. The final two columns give the expected number of events in LDMX assuming that ALPs originate only from the tungsten target with a thickness of 0.03504 cm. These numbers do not factor in the efficiency and acceptance of the experiment and our trigger/reconstruction algorithms.

In order to produce ALPs for the Primakoff process a sample of secondary photons, from electrons at the LDMX target, were extracted using LDMX-sw v14. A 8 GeV electron gun was fired into the tungsten target. Photons were collected at the back of the target and the spectrum of these photons was sampled and input into the ALP generator. To produce an ALP, the photon must have $E_\gamma \geq m_{ALP}$. This means we are more likely to produce lower mass ALPs and the majority of photons will be too soft to produce ALPs with viable masses. The fraction of soft photons unable to produce ALPs will increase with the mass of the ALP. Figure 1 shows the distribution of secondary photons from a 8 GeV electron beam, as measured at the back of the target. It should be noted that GEANT by default uses a model for bremsstrahlung that gives wrong predictions for electron bremsstrahlung (specifically the photon and electron momenta are correlated incorrectly - this gets washed out in thick targets, but it may be relevant for a thin target).

TODO: The production kinematics in the two processes are different. This will result in different detection efficiencies and different shower characteristics. This is something which needs to be looked at in detail (TODO)

2.1 Signal Yield Estimates

The number of ALPs we reconstruct in the experiment (N^{reco}_{ALP}) will be a product of a number of factors:

$$N^{reco}_{ALP\to\gamma}|_{proc.} = \mathcal{L} \cdot \sigma_{proc.} \cdot \epsilon_{reco} \cdot \epsilon_{trig.} \cdot \epsilon_{sel.} \tag{2}$$

where $\mathcal{L}$ is the effective luminosity, *proc.* refers to the production process (Primakoff or photon fusion), and σ_{proc} is the cross-section for a given ALP production, ϵ_{reco} is the fraction of ALP events which are reconstructed, $\epsilon_{trig.}$ is the fraction of ALP events that pass triggering algorithms and $\epsilon_{sel.}$ is the fraction of events passing any event selection cuts we enforce at analysis-level. This would include the S_{BDT} selection.

Expanding the luminosity factor gives:

$$N^{reco}_{ALP\to\gamma}|_{proc.} = N_{EoT} \cdot z \cdot \rho \cdot 10^{-36} \cdot \sigma_{proc.} \cdot \epsilon_{reco} \cdot \epsilon_{trig.} \cdot \epsilon_{sel.} \tag{3}$$

where $z = 0.0305$ cm is the target thickness, ρ is the number density for the tungsten in the target and 10^{-36} is a conversion factor. The combined factor $N_{EoT} \cdot z \cdot \rho \cdot 10^{-36} \cdot \sigma_{proc.}$ gives the number of ALPs for a given production mode. This term is collectively N^{prod}_{proc}

$$N^{reco}_{ALP\to\gamma}|_{proc.} = N^{prod}_{proc} \times \epsilon_{reco} \times \epsilon_{trig.} \times \epsilon_{sel.} \tag{4}$$

where $N^{prod}_{proc} = 0.22 \cdot \sigma_{proc.}$ for 1e14 EoT.

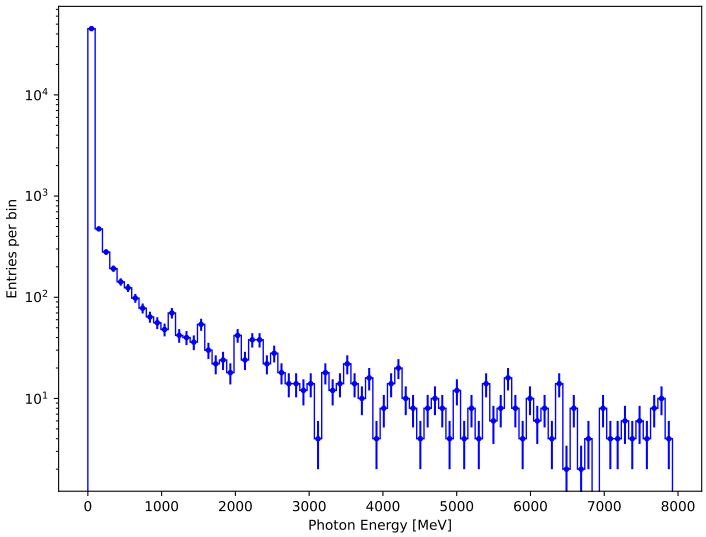

Figure 1: Secondary photons from 8 GeV electron beam as measured at the back of the tungsten target, made using LDMX-sw v14.

2.2 Cross-sections

Figure 2 shows how the cross-sections, derived using MadGraph, change as a function of the outgoing ALP mass. Both plots show the same structure, that higher mass signals are less likely to be produced. The cross-sections are an order of magnitude larger for the Primakoff case, this reflects the secondary photon yield. The Primakoff process will be dominant, as expected.

Table 1 lists the cross-sections as well as a derived number of expected events, assuming $N_{EoT} = 1 \times 10^{14}$ electrons in Phase I of LDMX. The acceptance and various efficiencies are not yet factored in, therefore these numbers are only presented for discussion purposes.

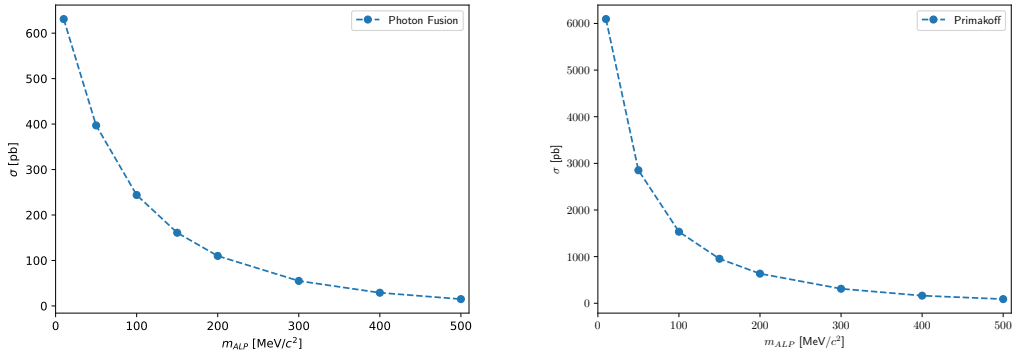

Figure 2: Cross-sections from MG4

Table 1: Cross-sections and expected number of events (assuming 1e14 Electrons on Target and that the ALPs are produced in the target only and that the target is 0.03504 cm thick Tungsten target)

$m_{ALP}[MeV/c^2]$	Phot. Fus. σ [pb]	Prima. σ [pb]	Phot. Fus. N_{proc}^{prod}	Prima. N_{proc}^{prod}
10	631	6094	139	1340
50	397	2852	87	627
100	244	1534	53	337
150	161	954	35	210
200	110	635	24	140
300	55	311	12	68
400	29	163	6	36
500	15	89	3	20

Table 2: Reconstruction Efficiency for Primakoff samples and expected yield (without factoring in selection or trigger) for 1e14 EoT.

$m_{ALP}[MeV]$	ϵ_{rec} [%]	expected yield
10	0	0
50	4	25
100	17	57
150	18	38
200	33	46
300	45	31
400	35	13
500	51	10

Table 3: Reconstruction Efficiency for photon fusion samples and expected yield (without factoring in selection or trigger) for 1e14 EoT

$m_{ALP}[MeV]$	ϵ_{rec} [%]	expected yield
10	15	21
50	9	8
100	16	8
150	15	5
200	17	4
300	26	3
400	20	1
500	20	0

2.3 Efficiencies

2.3.1 Reconstruction Efficiency

In this analysis we look at reconstructed information in the ECAL and HCAL but specifically focus on using the HCAL to distinguish photons from neutrons.

Tables 2 and 3 list the number of events that could be potentially reconstructed for a 1e14 8 GeV electron sample. These numbers incorporate only reconstruction efficiency. And event was classified as reconstructable if it produced HCAL recostructed hits, no filtering or selections were applied beyone this. They do not factor in selection efficiency if any cuts are applied.

TODO: these numbers should be double checked and uncertainties shown

3 Discriminating Signal and Background

TODO: retrain this BDT for complete dataset

3.1 Particle Guns

To understand the HCAL's ability to separate photons from neutrons, a general case of a photons and neutrons with energy $200 < E_{\gamma,n} < 2000$ MeV were simulated using simple particle guns in the LDMX-sw code base.

3.1.1 Features

The shower shapes were characterized and a simple Boosted Decision Tree (BDT) was constructed. The features included in this BDT were:

1. **NHits** - Number of Reconstructed HCAL Hits;
2. **ZAverage** - Average Longitudinal Position of Reconstructed HCAL Hits;
3. **ZWidth** - RMS of Longitudinal Positions of Reconstructed HCAL Hits;
4. **EDensity** - Energy deposited per unit length in Z;
5. **Eav** - Average Energy Deposited in Reconstructed HCAL Hits.

Only reconstructed quantities were used since only these will be derivable from real data. The BDT was written using ROOT's TMVA [4] framework. A Gradient BDT was chosen. Figure 3 shows the distributions of these features for signal (1GeV photon in this case) and background (1GeV neutron). All the chosen features provide some discrimination between the signal and background events. ZAverage has the largest discriminative power, followed by EDensity. The number of hits has least discriminative power. An initial sample of 10000 events is used wit ha 50:50 split used to test and train the BDT.

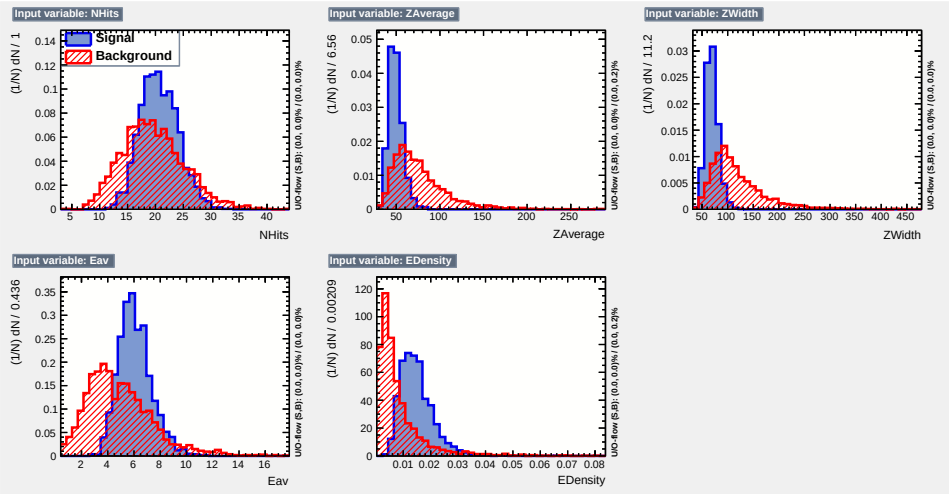

Figure 3: Features input into TMVA BDT for case where signal is a 1GeV photon and background is a 1GeV neutron

Figure 4 shows the correlation matrices for the signal (a photon of 1GeV) and background (a neutron of 1GeV). Several of the features are anti-correlated such as NHits and EDensity, this is to be expected. A longer track has more hits but a smaller energy deposited per hit.

The BDT was then trained sets of photons and neutrons of energies 200MeV, 500MeV, 1GeV and 2GeV. The resulting BDT Score (S_{BDT}) distributions are shown in figure 5. A selection criterion of

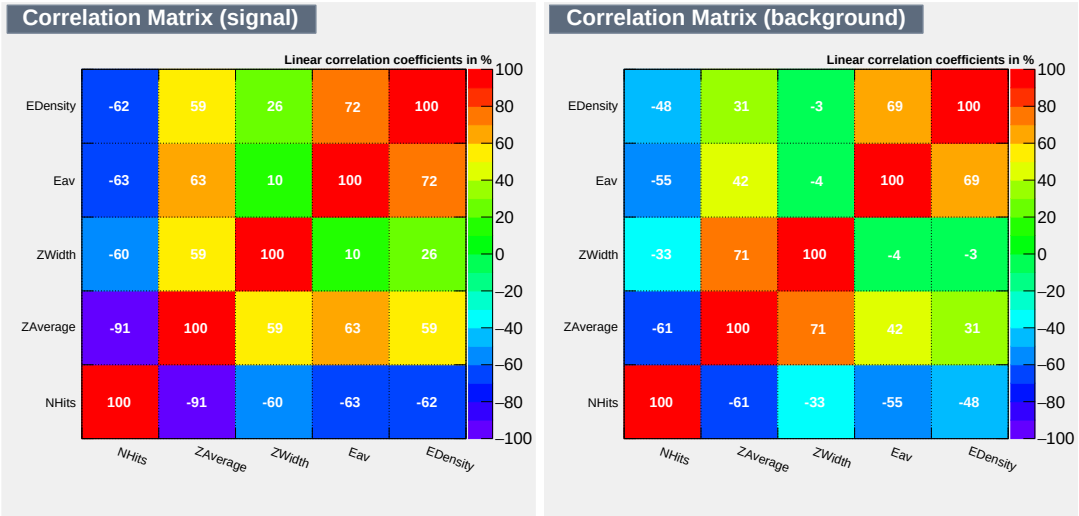

Figure 4: Correlation matrices for signal and background, for case where signal is a 1GeV photon and background is a 1GeV neutron

$S_{BDT} > 0.9$ results a signal efficiency of 68 % and a background efficiency of 0.9%. The purity of events in this region will therefore be less than the 1:100 requirement if we chose to enforce this criterion.

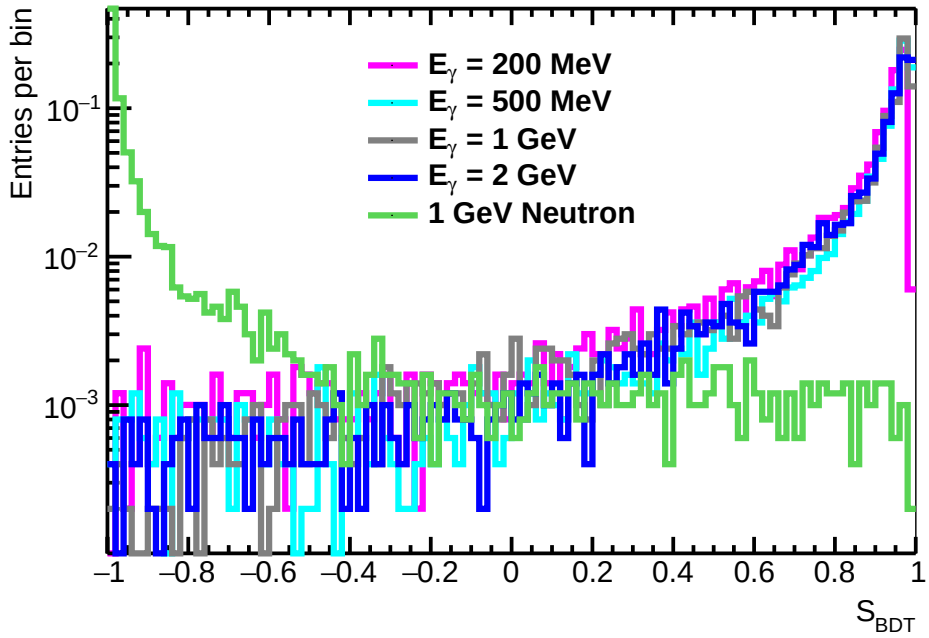

Figure 5: Distribution of BDT Scores for several photon gun samples, the background shown corresponds to a 1GeV neutron gun. Testing samples correspond to 5000 events. A logarithmic scale is used to accentuate the tail regions.

In conclusion, with this simple BDT a reasonable level of discrimination is possible with the simple photon/neutron guns. Further optimization of the BDT is probably a good idea and could provide better efficiencies, and possibly higher signal retention, but it is not necessary.

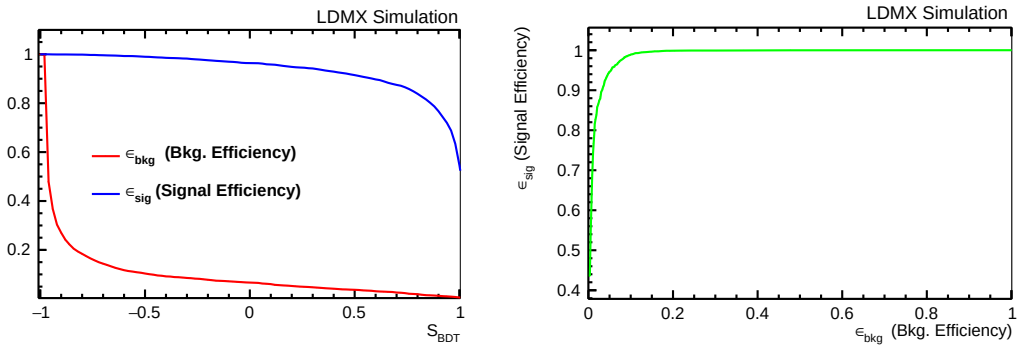

Figure 6: Changes in signal and background efficiency with S_{BDT}

3.2 Alternatives to TMVA

The same samples were passed through as a series of well-known classifiers. The python package sklearn was used to implement these classifiers. Figure 7 shows the accuracy of these classifiers for separating a 1GeV neutron (background) from a photon of a given energy (signal). The Support Vector Classifier (SVC) provides the highest accuracy for all energies. However, there is still as 4 % chance of wrongly identifying a background 1GeV neutron as a 1GeV photon.

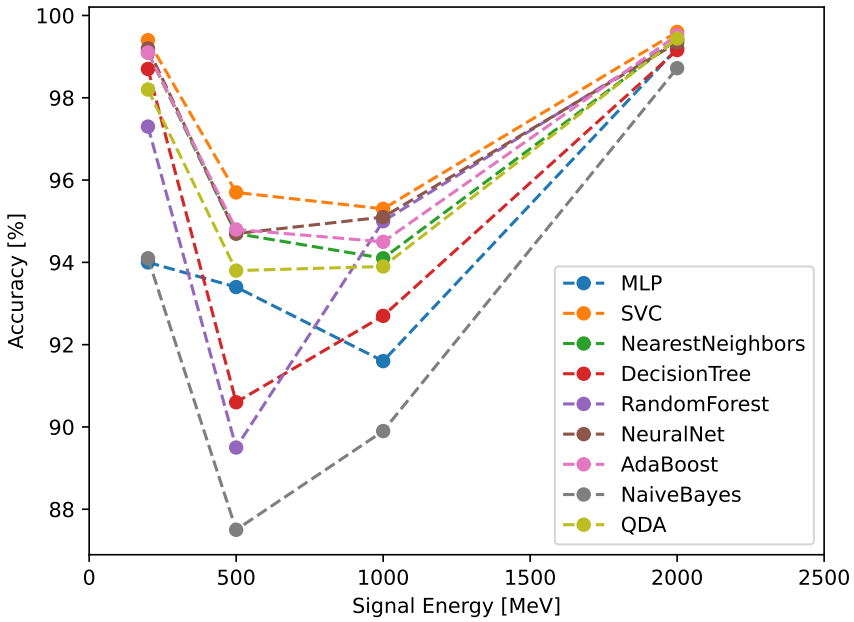

Figure 7: Responses of various sklearn classifiers for situations when the background is a 1GeV neutron and signal is a photon of a given energy.

3.3 Geometry Changes

To ensure we are optimal to look for ALPs using the HCAL a few geometry changes were made including altering the absorber thickness from 20 cm to 15 and 50 cm. Looking at just the particle guns, directly

in front of the back hcal, the reconstruction efficiency and BDT response is very similar to that with the nominal absorber thickness.

4 Selection Efficiency: Applying BDT to ALP and PN samples

Once the BDT is trained completely we must apply it to both the PN and ALP samples.

5 Expected Sensitivity

5.1 Background Optimization

5.2 Sensitivity

5.3 Further Study

References

[1] A. Ringwald, "*Axions and Axion-Like Particles*," 2014. https://arxiv.org/abs/1407.0546.

[2] A. Berlin, N. Blinov, G. Krnjaic, P. Schuster, and N. Toro Physical Review D **99** no. 7, (Apr, 2019) . https://doi.org/10.1103%2Fphysrevd.99.075001.

[3] J. Alwall and all, "*MadGraph/MadEvent v4: the new web generation*," Journal of High Energy Physics **2007** no. 09, (Sep, 2007) 028–028. https://doi.org/10.1088%2F1126-6708%2F2007%2F09%2F028.

[4] A. Hoecker *et al.*, "*TMVA - Toolkit for Multivariate Data Analysis*," 2007. https://arxiv.org/abs/physics/0703039.